FINDING HIGH-REDSHIFT DARK STARS WITH THE *JAMES WEBB SPACE TELESCOPE*

Erik Zackrisson[1,2], Pat Scott[2,3], Claes-Erik Rydberg[1,2], Fabio Iocco[4], Bengt Edvardsson[5], Göran Östlin[1,2],
Sofia Sivertsson[2,6], Adi Zitrin[7], Tom Broadhurst[7], and Paolo Gondolo[8]

[1] Department of Astronomy, Stockholm University, 10691 Stockholm, Sweden; ez@astro.su.se
[2] Oskar Klein Centre for Cosmoparticle Physics, AlbaNova University Centre, 10691 Stockholm, Sweden
[3] Department of Physics, Stockholm University, 10691 Stockholm, Sweden
[4] Institut d'Astrophysique de Paris, UMR 7095-CNRS Paris, Université Pierre et Marie Curie, Boulevard Arago 98bis, 75014, Paris, France
[5] Department of Physics and Astronomy, Uppsala Astonomical Observatory, Box 516, 751 20 Uppsala, Sweden
[6] Department of Theoretical Physics, Royal Institute of Technology (KTH), 10691 Stockholm, Sweden
[7] School of Physics and Astronomy, Tel Aviv University, Israel
[8] Physics Department, University of Utah, Salt Lake City, UT84112, USA
Received 2010 February 5; accepted 2010 May 2; published 2010 June 10

ABSTRACT

The first stars in the history of the universe are likely to form in the dense central regions of $\sim 10^5$–$10^6\ M_\odot$ cold dark matter halos at $z \approx 10$–50. The annihilation of dark matter particles in these environments may lead to the formation of so-called dark stars, which are predicted to be cooler, larger, more massive, and potentially more long-lived than conventional population III stars. Here, we investigate the prospects of detecting high-redshift dark stars with the upcoming *James Webb Space Telescope* (*JWST*). We find that all dark stars with masses up to $10^3\ M_\odot$ are intrinsically too faint to be detected by *JWST* at $z > 6$. However, by exploiting foreground galaxy clusters as gravitational telescopes do, certain varieties of cool ($T_{\mathrm{eff}} \leqslant 30{,}000$ K) dark stars should be within reach at redshifts up to $z \approx 10$. If the lifetimes of dark stars are sufficiently long, many such objects may also congregate inside the first galaxies. We demonstrate that this could give rise to peculiar features in the integrated spectra of galaxies at high redshifts, provided that dark stars make up at least $\sim 1\%$ of the total stellar mass in such objects.

Key words: dark ages, reionization, first stars – dark matter – galaxies: high-redshift – stars: Population III

Online-only material: color figures

1. INTRODUCTION

The first stars in the history of the universe are predicted to form inside $\sim 10^5$–$10^6\ M_\odot$ minihalos at redshifts $z \approx 10$–50 (e.g., Tegmark et al. 1997; Yoshida et al. 2003). Due to the lack of efficient coolants in the primordial gas at these early epochs, the resulting population III stars are believed to be very massive ($\gtrsim 100\ M_\odot$; e.g., Abel et al. 2002; Bromm et al. 2002), hot (effective temperature $T_{\mathrm{eff}} \sim 10^5$ K; e.g., Bromm et al. 2001), and short-lived (≈ 2–3 Myr; Schaerer 2002). Non-rotating population III stars with masses 50–140 $M_\odot$ or $M > 260\ M_\odot$ are expected to collapse directly to black holes, whereas stars with masses 140–260 $M_\odot$ may produce luminous pair-instability supernovae (e.g., Heger et al. 2002). The latter may enrich the ambient medium with heavy elements and initiate the transition to the normal mode of star formation (population I and II, with a characteristic stellar mass $<1\ M_\odot$) known from the low-redshift universe. The highly energetic radiation emitted from population III stars during their lifetimes may also have played an important role in cosmic reionization at $z > 6$ (e.g., Sokasian et al. 2004; Trenti & Stiavelli 2009). An observational confirmation of very massive population III stars would be an important breakthrough in the study of star formation, chemical enrichment, and reionization history of the universe.

The *James Webb Space Telescope*[9](*JWST*), scheduled for launch in 2014, has been designed to study the epoch of the first light, reionization, and galaxy assembly but is not expected to be able to directly detect individual population III stars at $z \gtrsim 10$. Searches for population III stars with *JWST* would instead focus

on the pair-instability supernovae produced at the end of their lifetimes (Weinmann & Lilly 2005) or on $\sim 10^5$–$10^7\ M_\odot$ clusters of population III stars (Bromm et al. 2001; Scannapieco et al. 2003; Trenti et al. 2009; Johnson et al. 2009; Johnson 2010). Other alternatives are to look for the spectral signatures of population III stars forming in pockets of unenriched gas within high-redshift galaxies (Tumlinson & Shull 2000; Schaerer 2002, 2003; Dijkstra & Wyithe 2007; Johnson et al. 2008) or their integrated contribution to the infrared extragalactic background light (Santos et al. 2002; Cooray et al. 2009).

It has recently been recognized that annihilation of dark matter in the form of weakly interacting massive particles (WIMPs; e.g., the lightest supersymmetric or Kaluza–Klein particles, or an extra inert Higgs boson) may have generated a first population of stars with properties very different from the canonical population III (Spolyar et al. 2008). Because the first stars are likely to form in the high-density central regions of minihalos, annihilation of dark matter into standard model particles could serve as an additional energy source alongside or instead of nuclear fusion within these objects. This leads to the formation of the so-called dark stars, which are predicted to be cooler, larger, more massive, and potentially longer-lived than conventional population III stars (Spolyar et al. 2008, 2009; Iocco 2008; Freese et al. 2008, 2009; Iocco et al. 2008; Yoon et al. 2008; Taoso et al. 2008; Natarajan et al. 2009; Umeda et al. 2009; Ripamonti et al. 2009). Similar effects have been seen in studies of the impacts of dark matter upon population I and II stars (Salati & Silk 1989; Fairbairn et al. 2008; Scott et al. 2008, 2009b; Casanellas & Lopes 2009).

A significant population of high-redshift dark stars could have important consequences for the formation of intermediate and supermassive black holes (Spolyar et al. 2009), for the cosmic

---

[9] http://www.jwst.nasa.gov

evolution of the pair-instability supernova rate (Iocco 2009), for the X-ray extragalactic background, and for the reionization history of the universe (Schleicher et al. 2009). Effects such as these can be used to indirectly constrain the properties of dark stars, but no compelling evidence for or against a dark star population at high redshifts has so far emerged. Here, we explore a more direct approach—the prospects for detection of population III dark stars using *JWST*.

While attempting to assess the detectability of dark stars at high redshifts, the expected lifespan of such objects represents a crucial aspect. In principle, dark stars could live indefinitely, provided that there is ample dark matter available to fuel them. Dark stars are powered by gravitationally contracted dark matter and pulled into their core as infalling gas steepens the gravitational potential during the formation phase. Because annihilation depletes the dark matter present within a star, ordinary fusion processes eventually take over as the dominant power source if the dark matter is not replenished. At this point, the dark star will essentially transform into a conventional population III star, albeit more massive because the increased duration of the formation phase has allowed it to accrete more gas. The dark matter present within the star during formation will last only for a few million years, but these reserves may later be replenished by scattering of WIMPs on nucleons, causing them to lose energy and become captured in the stellar core. This could boost the longevity of dark stars substantially (Iocco et al. 2008; Freese et al. 2008; Yoon et al. 2008; Taoso et al. 2008; Spolyar et al. 2009; Iocco 2009). The ongoing replenishment of the dark matter through capture and the resultant increase in longevity rely upon a number of strong assumptions and approximations, and the feasibility of such a mechanism is still yet to be proven by detailed calculations (S. Sivertsson & P. Gondolo 2010, in preparation).

Whether the capture process will be efficient depends on two factors: the scattering cross sections of the dark matter particles with ordinary nucleons and the amount and density of dark matter available for capture from the star's surroundings. The WIMP-nucleon scattering cross sections can be constrained by direct detection experiments (e.g., Savage et al. 2009; Ahmed et al. 2009) and searches for neutrinos produced by annihilation in the Sun (e.g., Abbasi et al. 2009). However, the question of the amount of dark matter available for refueling is more complicated (S. Sivertsson & P. Gondolo 2010, in preparation). In a pristine halo, WIMP annihilations and scatterings during the formation stage would eventually deplete orbits with low angular momenta and result in a cavity of reduced dark matter density in the vicinity of the dark star. Whether infalling WIMPs could restore the balance before the star evolves into a supernova or a black hole may depend on the overall structural evolution of the minihalo (e.g., contraction, mergers with other halos) and on tidal interactions of the dark star with subhalos, gas clouds, and possibly other population III stars within the minihalo itself. Should a violent event cause the dark star to venture far from the center of the minihalo, the dark matter density would very quickly become too low to sustain further dark matter burning. At the current time, estimates of the dark star lifetime in the presence of capture range from a few times 10^5 to 10^{10} yr (e.g., Yoon et al. 2008; Iocco 2009; S. Sivertsson & P. Gondolo 2010, in preparation). Many of the mechanisms mentioned above for replenishing the dark matter in the center of the dark star have moreover not yet been explored. In this paper, we will therefore treat the duration of the dark star phase as a free parameter.

Model atmospheres and evolutionary histories of dark stars are presented in Section 2. The detectability of isolated dark stars, with and without the effects of gravitational lensing by foreground galaxy clusters, is explored in Section 3. In Section 4, we explain how high-redshift dark stars can be distinguished from other objects based on their *JWST* colors and discuss the possibility of detecting the spectral signatures of dark stars in the first generations of galaxies. Section 5 summarizes our findings. Throughout this paper, we will assume a ΛCDM cosmology with $\Omega_\Lambda = 0.73$, $\Omega_M = 0.27$, and $H_0 = 72$ km s^{-1} Mpc^{-1}.

After this paper had been submitted, another paper (Freese et al. 2010) dealing with the prospects of detecting high-redshift dark stars with the *JWST* was posted on the arXiv preprint server. The two studies differ in their assumptions concerning the masses of dark stars. Whereas we consider objects with masses up to $\sim 10^3$ $M_\odot$, Freese et al. instead focus on the detectability of "supermassive dark stars" (with masses up to 10^7 $M_\odot$).

2. MODELS FOR DARK STARS

2.1. Stellar Structure and Evolution

As described in the previous section, two physical processes exist for bringing dark matter into a star: gravitational contraction and capture by nuclear scattering. Studies of the structure, formation, and evolution of dark stars have so far employed one of two simulation techniques: either a "formationary" or a "hydrostatic" approach. In general, either physical process (or both) can be included with either simulation technique. Most studies to date employing the formationary approach have included only gravitational contraction, whereas most studies following the hydrostatic approach have included only capture by nuclear scattering. There are, however, notable examples of both hydrostatic (Iocco et al. 2008) and formationary (Spolyar et al. 2009) studies which include both physical processes.

The formationary approach follows the initial collapse of the pre-stellar gas cloud, the resultant gravitational contraction of its dark matter halo, and the subsequent formation of the dark star (Spolyar et al. 2008, 2009; Freese et al. 2008; Natarajan et al. 2009; Ripamonti et al. 2009, 2010). This approach captures the salient points of dark star formation and early evolution, which are primarily governed by the annihilation of the gravitationally contracted dark matter. The strategy is not optimized for dealing with the stellar evolution after formation, because it relies on either full hydrodynamic simulations (Natarajan et al. 2009; Ripamonti et al. 2009, 2010) or analytical approximations to them (Spolyar et al. 2008, 2009), becoming either too numerically demanding or reliant upon simple polytropes once the star has condensed.

The hydrostatic approach assumes some initial model for either a main-sequence (Scott et al. 2008, 2009b; Yoon et al. 2008; Taoso et al. 2008; Casanellas & Lopes 2009) or pre-main-sequence star (Iocco et al. 2008; Umeda et al. 2009; Casanellas & Lopes 2009). This model is then run through a modified quasi-hydrostatic stellar evolution code (e.g., Scott et al. 2009a) and evolved with the inclusion of energy injection by WIMP annihilation. Late-stage evolution is typically dominated by dark matter distribution outside the star and the resultant rate at which WIMPs are captured by the nuclear scattering process. Progress has been made in including some early-stage effects, like gravitationally contracted dark matter (Iocco et al. 2008) and gas accretion (Umeda et al. 2009), but the realism of such simulations ultimately suffers from their inability to deal with times before hydrostatic equilibrium is reached.

For our purposes, the most significant finding in hydrostatic studies was the possibility that the lifetimes of dark stars might be extended. In this situation, WIMP-dominated models "stall" (either temporarily or permanently) when they reach an equilibrium configuration somewhere on the Hayashi track (Fairbairn et al. 2008; Scott et al. 2008; Iocco et al. 2008; Yoon et al. 2008; Taoso et al. 2008). For a given stellar mass, the position is essentially dependent only on the WIMP capture rate (Scott et al. 2009b) and does not depend strongly on whether simulations are started from the main or pre-main sequence (Casanellas & Lopes 2009).

The formationary approach produces more realistic protostellar structures, whereas the hydrostatic one allows more accurate modeling of long-term evolution. It is likely that the results of more sophisticated simulations, where formation and later quasi-hydrostatic evolution are treated self-consistently and detailed capture calculations are also included, would resemble a superimposition of the hydrostatic results upon the formationary ones. Depending upon the time required for dark matter captured by nuclear scattering to become a significant contributor to a star's energy budget, three outcomes are possible.

1. The star may stall directly on the evolutionary paths described by Spolyar et al. (2009) during its march toward the main sequence.
2. The star may contract onto the zero-age main sequence (ZAMS) as per the Spolyar et al. (2009) paths and then re-inflate as annihilation of captured dark matter pushes it back up the Hayashi track.
3. The star might travel only some of the way to the ZAMS but then be turned around and partially re-inflate as the captured dark matter asserts itself.

Scenario 1 would typically be associated with a very quick onset of annihilation from dark matter captured by nuclear scattering, 2 would result if capture takes a very long time to assert itself, and 3 is an intermediate scenario. The amount of time the captured population takes to become significant is most sensitive to the total capture rate, also to the time required for equilibrium to be achieved between capture and annihilation, and the time required for WIMPs to thermalize inside the star. These quantities in turn depend very strongly on the adopted models for the WIMP particle (mass, annihilation cross section and scattering cross section) and the dark matter halo (density and velocity structure). In particular, these dependencies are rather degenerate; the impact of a short equilibrium timescale can, for example, be mimicked by a denser dark matter halo. This picture is further complicated by the fact that accretion may also continue to some degree in scenarios 1 and 3, because it may not have been halted by radiative feedback when the star draws close to the main sequence. The more massive a star becomes, the more dark matter is needed to keep it from contracting onto the main sequence.

Where in the H-R diagram a stalled configuration occurs, depends upon the total capture rate of dark matter; different annihilation rates are required to support an equilibrium structure at different locations on the Hayashi track. For a fixed stellar mass, greater rates of capture are required to support a star further from ZAMS, i.e., at earlier stages in its contraction. However, larger stellar masses require substantially higher capture rates, so in realistic formation scenarios this effect will be countered to some degree by accretion. Which effect dominates, depends upon the actual accretion rate during the formation phase.

How long the stalling phase persists is determined by the timescale over which the star's hydrogen remains undepleted at a given position on the Hayashi track and how long capture can be realistically maintained at the given rate. The hydrogen-burning timescale is a function of the central temperature and density of the star (i.e., the position on the Hayashi track) and is therefore also a function of the capture rate. At low capture rates, nuclear burning takes over relatively quickly regardless of how long capture continues, whereas at high capture rates it can in principle remain suppressed (or even entirely absent) for an indefinite period, unless capture drops because the WIMP halo has been depleted.

For very low capture rates—where stars stall only very briefly near the main sequence (e.g., very late on the Spolyar et al. 2009 tracks)—the longest possible lifetime of a dark star is set by the hydrogen-burning lifetime. This is the approximate maximum time $t_{\rm burn}$ that it would take for all the core hydrogen to be converted to helium, if the star were not to contract any further. For normal Pop III stars, this is set by the timescale in which hydrogen will be depleted by CNO-cycle burning, as helium burning by the triple alpha process quickly creates sufficient C, N, and O to catalyze the cycle and allow it to outstrip hydrogen burning by the pp-chain. In the case of dark stars however, depending upon how close to ZAMS any stalling phase occurs, the triple alpha process may not become relevant until rather late. In this case, the hydrogen-burning lifetime will be given by the rate-limiting step of the pp-chain ($p + p \rightarrow d + e^+ + \nu_e$), such that

$$t_{\rm burn} = \frac{1}{2 m_p r_{\rm pp}(T_{\rm c}, \rho_{\rm c})}. \tag{1}$$

Here, m_p is the proton mass, $T_{\rm c}$ and $\rho_{\rm c}$ are the central temperature and density of the star, and $r_{\rm pp}$ is the nuclear reaction rate, given in Cox (2000). For dark stars stalled close to ZAMS, the true hydrogen-burning lifetime will likely be somewhat shorter, due to the effectiveness of the CNO cycle. The simulations of Spolyar et al. (2009) did not, however, take into account evolution in the stellar chemical composition, so estimating the time-varying rate of CNO-cycle hydrogen burning in the stars we consider is not completely straightforward. Here, we choose to apply only the pp-chain limit, as this is a hard limit in the sense that it cannot be evaded by arguments about the stellar model-dependence of any CNO abundances we might derive.

For very high capture rates, the longest plausible lifetime of a dark star is instead set by the time required for the surrounding dark matter density to drop below that required to sustain the star, due to self-annihilation in the halo. Once the density of the halo is lowered, capture is reduced and the star contracts and gradually moves onto the main sequence. The halo density required to power a dark star of a given mass and luminosity can be estimated using Equation (14) in Iocco et al. (2008). The self-annihilation time $t_{\rm SA}$ for a halo with a given dark matter density can then be obtained by, e.g., inverting Equation (6) in Scott & Sivertsson (2009). The self-annihilation times obtained in this manner are rather approximate, relying on a number of assumptions we already know to be violated in the first stars (a constant halo self-annihilation rate and the constant infall of WIMPs from a uniform, unbound dark matter halo with an assumed velocity structure). A more conservative approach, which is thus also much less dependent on the adopted halo model, is to take the corresponding upper limit on stellar lifetimes to be $\sim 100\, t_{\rm SA}$, which is the strategy adopted in this paper. The factor of 100 results from an approximate order-of-magnitude uncertainty from the constant annihilation rate

Table 1
Dark Star Models

WIMP Mass	M ($M_\odot$)[a]	R (cm)[a]	$\log_{10}(g)$[b]	$T_{\rm eff}$ (K)[a]	$t_{\rm burn}$ (yr)	$t_{\rm SA}$ (yr)	$t_{\rm max}$ (yr)	Atmosphere	max($z_{\rm obs}$)[c]
1 GeV	106	2.4×10^{14}	-0.612	5.4×10^3	$> 10^{10}$	2.0×10^5	2.0×10^7	MARCS	10
	371	2.7×10^{14}	-0.170	5.9×10^3	$> 10^{10}$	1.2×10^6	1.2×10^8	MARCS	11
	690	1.1×10^{14}	0.879	7.5×10^3	$> 10^{10}$	2.4×10^7	5.0×10^8	MARCS	11
	756	3.7×10^{13}	1.865	1.0×10^4	$> 10^{10}$	2.3×10^8	5.0×10^8	TLUSTY	9
	793	5.7×10^{12}	3.511	3.0×10^4	$> 10^{10}$	8.7×10^8	5.0×10^8	TLUSTY	11
	824	5.8×10^{11}	5.512	1.1×10^5	6.2×10^6	4.9×10^9	6.2×10^6	TLUSTY	0.5
100 GeV	106	7.0×10^{13}	0.458	5.8×10^3	$> 10^{10}$	6.0×10^6	5.0×10^8	MARCS	6
	479	8.4×10^{13}	0.955	7.8×10^3	$> 10^{10}$	2.2×10^7	5.0×10^8	MARCS	11
	716	1.1×10^{13}	2.895	2.3×10^4	$> 10^{10}$	2.9×10^8	5.0×10^8	TLUSTY	13
	756	2.0×10^{12}	4.399	5.5×10^4	2.2×10^9	1.6×10^9	5.0×10^8	TLUSTY	3
	787	5.8×10^{11}	5.492	1.1×10^5	5.9×10^6	4.5×10^9	5.9×10^6	TLUSTY	0.5
10 TeV	106	2.2×10^{13}	1.463	6.0×10^3	$> 10^{10}$	1.7×10^8	5.0×10^8	MARCS	2
	256	2.2×10^{13}	1.846	8.0×10^3	$> 10^{10}$	3.1×10^8	5.0×10^8	MARCS	4
	327	2.0×10^{13}	2.036	1.0×10^4	$> 10^{10}$	2.8×10^8	5.0×10^8	TLUSTY	5
	399	6.6×10^{12}	3.085	2.5×10^4	$> 10^{10}$	2.9×10^8	5.0×10^8	TLUSTY	7
	479	2.9×10^{12}	3.879	3.2×10^4	$> 10^{10}$	1.9×10^9	5.0×10^8	TLUSTY	2
	550	6.0×10^{11}	5.307	9.5×10^4	1.3×10^7	3.6×10^9	1.3×10^7	TLUSTY	0.5
	553	4.8×10^{11}	5.503	1.1×10^5	5.1×10^6	3.9×10^9	5.1×10^6	TLUSTY	< 0.5

Notes.
[a] From Spolyar et al. (2009).
[b] In units of g cm^{-1} s^{-2}.
[c] This observability limit is set by the requirement that a single dark star should be sufficiently bright in at least one *JWST* filter to give a 5σ detection after a 100 h exposure, if a gravitational magnification of $\mu = 160$ is assumed (see Section 3).

assumption, and the roughly order of magnitude change seen by Scott et al. (2009b) in capture rates from WIMP halos with alternative velocity distributions.

The capture and evolutionary histories of the first stars are clearly very dependent upon the adopted dark matter particle and halo models. To parameterize these uncertainties, as a simple approximation we consider models stalling at various positions on the evolutionary tracks of Spolyar et al. (2009). These models occupy similar positions in the H-R diagram to those computed from the ZAMS starting models (e.g., Iocco et al. 2008), despite the rather different physical interpretation of the two scenarios. We allow stars to stall at various positions on these tracks for times of up to $t_{\rm stall} = 5 \times 10^8$ yr. This upper limit roughly corresponds to the highest lifetimes considered realistic by Iocco (2009). To also take into account the effects of nuclear burning and halo self-annihilation, we limit the plausible lifetimes for any given model to values below

$$t_{\rm max} = \min(t_{\rm stall}, t_{\rm burn}, 100\, t_{\rm SA}). \qquad (2)$$

The parameters for these models are listed in Table 1.[10] This age span allows dark stars forming as early as $z = 30$ to survive until $z \approx 10$, and those forming as late as $z = 10$ to survive until the end of reionization ($z \approx 6$). In 5×10^8 yr, the minihalos hosting dark stars are likely to experience many mergers with other minihalos (typically once every $\sim 10^7$ yr; Greif et al. 2008). However, it is not clear whether this prevents or facilitates the existence of long-lived dark stars. Mergers may cause the dark star to be ejected from the center of the halo, thereby cutting off the supply of WIMPs, but may also channel fresh dark matter

into the halo center. In principle, one could even consider dark stars with lifetimes in excess of 5×10^8 yr (e.g., Freese et al. 2010), perhaps even dark stars surviving into the present-day era, but since *JWST* is probably not the optimal telescope for constraining such models, we will not consider them any further in this paper.

Here, we consider models computed with three different WIMP masses (1 GeV, 100 GeV, and 10 TeV) in the "minimal capture" approximation of Spolyar et al. (2009) in which WIMP annihilation and nuclear fusion contribute equally to the total stellar luminosity; further details can be found in that paper.

2.2. Model Atmosphere Spectra

To compute the expected spectral energy distributions (SEDs) of dark stars, we have used the MARCS stellar atmosphere code (Gustafsson et al. 2008) for $T_{\rm eff} \leqslant 8000$ K objects and the TLUSTY code (Hubeny & Lanz 1995) for $T_{\rm eff} \geqslant 10{,}000$ K. Since neither code is able to handle objects in the $T_{\rm eff} \approx 8000$–$10{,}000$ K range, we have interpolated the evolutionary tracks to produce replacement points just outside this temperature region whenever possible. In a few cases, it turned out to be necessary to adopt surface gravities $\log(g)$ slightly different from those given by the Spolyar et al. (2009) track to get convergence from MARCS. Neither the omission of the $T_{\rm eff} \approx 8000$–$10{,}000$ K data points nor the $\log(g)$ deviations have any significant impact on the results of this paper.

Provided that the properties of dark matter allow the formation of dark stars, objects of this type are expected to be among the first stars forming in the history of the universe and therefore to have extremely low metallicities Z, possibly at the level given by Big Bang nucleosynthesis (this implies $Z \sim 10^{-9}$ mainly due to Li; e.g., Iocco et al. 2007). All models therefore assume primordial abundances of H and He. For computational reasons, the MARCS atmospheres assume an overall metallicity of $Z = 2.5 \times 10^{-7}$ (corresponding to [Fe/H] $= -5$ with the α-enhanced abundance ratios discussed in Gustafsson et al.

---

[10] Due to convergence problems with the stellar atmosphere models for certain combinations of parameter values, the 100 GeV WIMP track in Table 1 has one data point less than the track in Spolyar et al. (2009). This does not have any impact on the results of the present paper, since the parameter space sampling of the converged models is more than sufficient to reveal the overall trends in magnitude and color evolution. The 10 TeV WIMP track also contains one data point more than the Spolyar et al. track to better bracket the 8000–10,000 K divide.

2008), whereas the TLUSTY have been computed at $Z = 0$. Tests indicate that this minor inconsistency amounts to an uncertainty in the final *JWST* magnitudes of ∼0.01 mag, which is irrelevant for the present study.

The TLUSTY models cover the rest-frame wavelength range 0.015–300 μm, whereas the MARCS model cover 0.13–20 μm. While parts of the spectra at wavelengths shortward of 0.13 μm may be redshifted into the range of the *JWST* detectors (0.6–29 μm) at $z > 4$, the fluxes in this part of the spectra are too small for detection in the case of cool dark stars. The wavelength coverage of our MARCS models is therefore more than adequate for our needs.

In the case of the hotter TLUSTY dark stars, corrections for foreground absorption need to be applied at wavelengths shortward of Lyα (0.1216 μm). At these wavelengths, the intergalactic medium becomes increasingly non-transparent at high redshifts due to H I absorption (Madau 1995), eventually turning almost completely opaque at $z > 6$ (e.g., Fan et al. 2006). To simulate this, all TLUSTY fluxes at $\lambda < 0.1216$ μm are set to zero whenever $z > 6$ but left unattenuated at lower redshifts. While this treatment may be too crude at lower redshifts (Madau 1995), this is not a major concern for the current study, which focuses on the prospects of detecting dark stars at $z > 6$.

As dark stars evolve along the Spolyar et al. (2009) tracks, they eventually attain temperatures similar to those of conventional population III stars (∼10^5 K) and photoionize large volumes of gas in their surroundings. The resulting H II regions will contribute emission lines and a nebular continuum to the overall spectra of such stars (Schaerer 2002, 2003), but this is not taken into account by our models. Because of this, the fluxes that we predict for the hottest dark stars should be considered conservative.

To obtain *JWST* magnitudes, all model spectra have been convolved with the transmission profiles for the broadband filters available for the NIRCam (0.6–5 μm) and MIRI (5–29 μm) instruments and calibrated using the AB system. This calibration, which will be used throughout this paper, is based on physical fluxes and defined so that an object with a constant flux per unit frequency interval of 3631 Jy has zero AB magnitudes m_{AB} in all filters.

The rest-frame stellar atmosphere spectra as well as the AB magnitudes (as a function of redshift from $z = 0$ to $z = 20$ in steps of $\Delta z = 0.5$) for the dark star models of Table 1 are available in electronic format through the VizieR service at CDS.[11]

3. THE DETECTABILITY OF HIGH-REDSHIFT DARK STARS

3.1. Dark Stars in Random Fields

In Figure 1, we present the AB magnitudes of all dark star models from Table 1 as a function of redshift ($z = 1$–20) in the NIRCam F444W filter. Also included are two estimated *JWST* detection thresholds for point sources, indicated by dashed horizontal lines. The first one is based on 10σ detections for 10^4 s exposures (thick dashed) and the second on 5σ detections after 100 h (3.6 × 10^5 s) exposures (thin dashed). The former represents the fiducial *JWST* detection limits listed on the *JWST* homepage,[12] whereas the latter roughly corresponds to the magnitude limits expected for "ultra deep field" type observations.
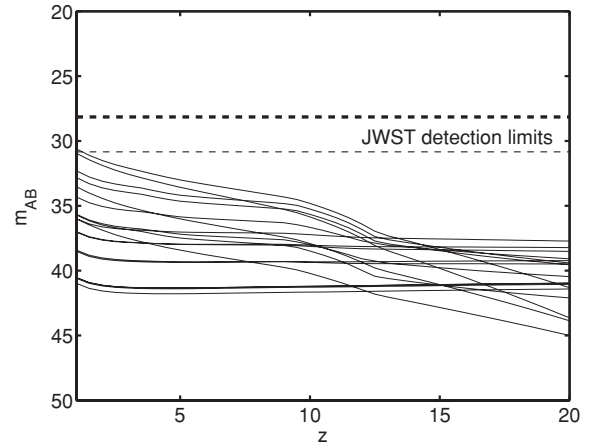
Figure 1. Predicted apparent AB magnitudes of dark stars at $z = 1$–20 in the NIRCam/F444W filter. Each solid line corresponds to a separate dark star model from Table 1. The dashed horizontal lines correspond to the *JWST* detection limits for a 10σ detection of a point source after 10^4 s of exposure (thick dashed) and for a 5σ detection of a point source after 3.6 × 10^5 s (100 hr) of exposure (thin dashed). At $z = 10$–20, the dark stars are 4–14 mag too faint for detection. Hence, without the magnification boost of a foreground galaxy cluster, *JWST* will not be able to detect individual population III dark stars at the redshifts where they formed. Long-lived dark stars surviving until the end of reionization ($z \approx 6$) appear somewhat brighter but are still at least 2 mag below the detection limit.

It is immediately clear that all dark star models lie significantly below both these detection thresholds at high redshifts. At $z = 10$–20, the intrinsic luminosities of the dark stars convert into apparent magnitudes that are 4–14 mag too faint. Hence, without the magnification boost of a foreground galaxy cluster, *JWST* will not be able to detect individual population III dark stars at the redshifts where they formed. Long-lived dark stars surviving until the end of reionization ($z \approx 6$) appear somewhat brighter but are still at least 2 mag below the detection limit.

Some of the dark star models in Figure 1 exhibit F444W magnitudes which change very little as a function of redshifts. This is due to the steep spectra of the $T_{eff} > 20,000$ K dark stars, which attain their peak fluxes at rest wavelengths <0.2 μm (i.e., on the short-wavelength side of the F444W filter for all redshifts in the plotted range). As the redshift is increased, intrinsically brighter parts of their spectra are redshifted into the F444W filter and this almost exactly compensates for the increased luminosity distance.

In Figure 2, we display AB magnitudes for all dark stars from Table 1 at $z = 6$ and $z = 10$ as a function of the central wavelengths of all broad *JWST* filters. The *JWST* detection limits, defined as in Figure 1, are also included. All dark star models from Table 1 lie significantly faintward of these thresholds, regardless of which filter is used. However, a magnification of $\mu = 160$ due to gravitational lensing by a foreground galaxy cluster (see Section 3.2) would shift all models upward by ≈5.5 mag (as indicated by the vertical arrow) and shift certain varieties of dark stars into the brightness regime detectable by the NIRCam instrument (but not by MIRI). This is the case for several of the $T_{eff} \leqslant 8000$ K dark stars (red lines; thin solid lines in the print version) and a couple of the 8000 K $< T_{eff} \leqslant 30,000$ K dark stars (green lines; thick solid lines in the print version) at both $z = 6$ and $z = 10$.

In Figure 3, we demonstrate the need for using synthetic stellar atmosphere spectra (as compared to pure blackbody spectra) for predictions of this type. In Figure 3(a), the MARCS spectra for the $106\,M_\odot$ ($T_{eff} = 5400$ K) dark star and the
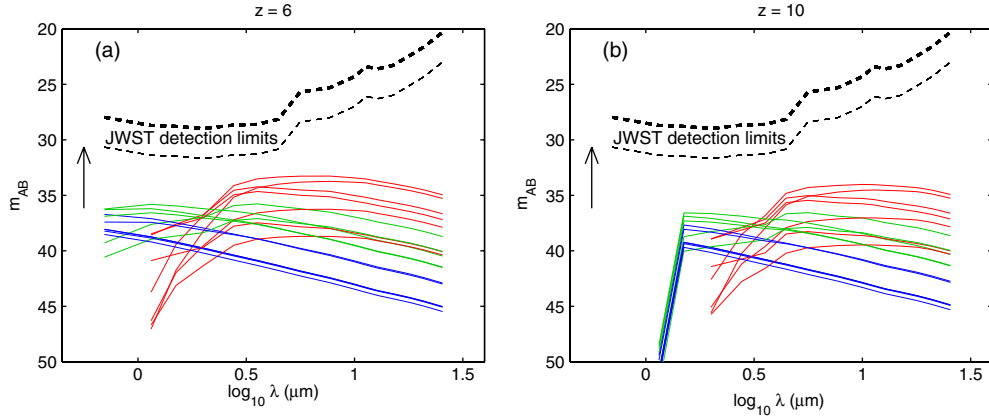
Figure 2. Predicted apparent AB magnitudes of dark stars at $z = 6$ (panel a) and $z = 10$ (panel b) as a function of central wavelength of the *JWST* broadband filters. Each solid line corresponds to a separate dark star model from Table 1. These lines have been color-coded according to the effective temperatures of the dark stars: $T_{eff} \leqslant 8000$ K (red; thin solid lines in the print version), 8000 K $< T_{eff} \leqslant 30{,}000$ K (green; thick solid lines in the print version), and $T_{eff} > 30{,}000$ K (blue; dot-dashed lines in the print version). The dashed horizontal lines correspond to the *JWST* detection limits for a 10σ detection of a point source after 10^4 s of exposure (thick dashed) and for a 5σ detection of a point source after 3.6×10^5 s (100 hr) of exposure (thin dashed). The progressively brighter detection thresholds at central wavelengths higher than 4.4 μm ($\log_{10} \lambda > 0.65$) reflect the lower sensitivity of the MIRI instrument (central filter wavelengths $\log_{10} \lambda > 0.65$) compared to NIRCam (central filter wavelengths $\log_{10} \lambda \leqslant 0.65$). In both panels, all dark star models lie significantly faintward of the detection thresholds in all filters, implying that their intrinsic brightnesses are too low to be detected by *JWST*. However, a magnification of $\mu = 160$ due to gravitational lensing by a foreground galaxy cluster (see Section 3.2) would shift all models upward by 5.5 mag (as indicated by the vertical arrow) and allow certain varieties of dark stars into the brightness regime detectable by the NIRCam instrument. This is the case for some of the $T_{eff} \leqslant 30{,}000$ K dark stars (green (thick solid) and red (thin solid) lines) at both $z = 6$ and $z = 10$. The reason why the red (thin solid) lines end abruptly at 1.15 μm ($\log_{10} \lambda = 0.06$) for $z = 6$ and at 2.0 μm ($\log_{10} \lambda = 0.3$) for $z = 10$ is that the short-wavelength limit (0.13 μm) of the MARCS model spectra has entered the bluer filters at these redshifts. Since this happens at $m_{AB} > 38$, which is a brightness regime inaccessible to the *JWST*, this has no impact on the present study. The sharp drop in brightness at $\lambda \leqslant 1.5$ μm ($\log_{10} \lambda \leqslant 0.17$) along the blue (dot-dashed) and green (thick solid) lines at $z = 10$ is due to H I absorption in the foreground intergalactic medium.

(A color version of this figure is available in the online journal.)
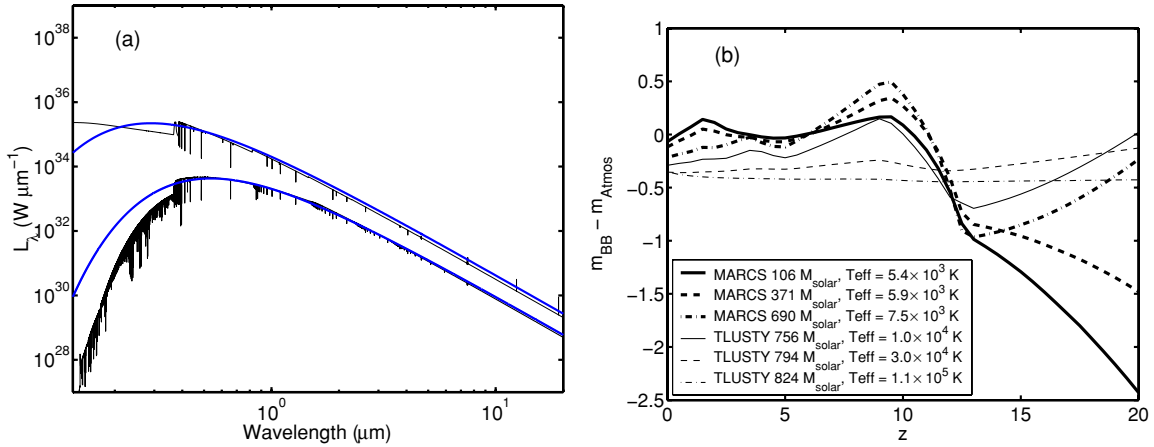

Figure 3. Synthetic stellar atmosphere spectra compared to blackbody spectra for dark stars. Panel (a): the SEDs of the 106 $M_{\odot}$, $T_{eff} = 5400$ K (lower SEDs), and the 756 $M_{\odot}$, $T_{eff} = 10{,}000$ K (upper SEDs, multiplied by 100 to avoid cluttering) dark stars predicted for a 1 GeV WIMP. The black lines correspond to the synthetic stellar atmosphere SEDs generated by MARCS (for the lower $T_{eff} = 5400$ K spectra) and TLUSTY (for the upper $T_{eff} = 10{,}000$ K spectra), whereas the blue lines correspond to blackbody spectra generated for identical temperatures and bolometric luminosities. The obvious differences are the lack of breaks (most notable at ≈ 0.36 μm) and absorption lines in the blackbody spectra. Due to the low but non-zero metallicity ([Fe/H] $= -5$) of the MARCS spectrum for the 106 $M_{\odot}$, $T_{eff} = 5400$ K dark star, numerous metal lines are seen shortward of 0.36 μm in the lower SED. While these lines appear to be strong due to the high spectral resolution of the model spectrum, they actually have very small equivalent widths and negligible impact on the *JWST* broadband fluxes. Panel (b): the difference between the blackbody AB magnitudes m_{BB} and the synthetic stellar atmosphere AB magnitudes m_{Atmos} in the NIRCam F444W filter. The different lines represent the six dark star models from Table 1 for a 1 GeV WIMP. The solid lines correspond to the MARCS (thick line) and TLUSTY (thin lines) dark star SEDs plotted in panel (a). There are substantial differences between m_{BB} and m_{Atmos} for the cooler ($\lesssim 10{,}000$ K) dark stars, whereas the differences for hotter dark stars are below 0.5 mag. This is primarily because the hotter stars become progressively more blackbody-like at the relevant wavelengths. For instance, the 0.36 μm break (which gives rise to the negative $m_{BB} - m_{Atmos}$ at $z \gtrsim 9$) is far less prominent for hotter objects.

(A color version of this figure is available in the online journal.)

TLUSTY spectra for the 756 $M_{\odot}$ ($T_{eff} = 10{,}000$ K) dark star from the 1 GeV WIMP track in Table 1 are compared to blackbody spectra based on identical temperatures and bolometric luminosities. At rest-frame wavelengths of $\lambda > 0.4$ μm, the shape of the continua is very similar for the stellar atmosphere and blackbody SEDs, but the presence of breaks in

the stellar atmosphere spectra (most notably the Balmer break at $\lambda \approx 0.36$ μm) will introduce substantial differences once these are redshifted into the *JWST* filters. The stellar atmosphere SEDs also contain a large number of absorption lines, but these will have far smaller effect of the broadband fluxes discussed here. In Figure 3(b), we show the difference between the

magnitudes derived from blackbody and the synthetic stellar atmosphere spectra in the NIRCam F444W filter. The different lines represent six dark star models from Table 1 for a WIMP mass of 1 GeV. The solid lines correspond to the MARCS (thick lines) and TLUSTY (thin lines) dark star SEDs plotted in Figure 3(a). As seen, there are substantial differences for the cooler ($\lesssim$10,000 K) dark stars, whereas the differences for hotter dark stars are below 0.5 mag. This is primarily because the hotter stars become progressively more blackbody-like at the relevant wavelengths. For instance, the 0.36 μm break (which makes the blackbody spectra overpredict the F444W fluxes at $z \gtrsim 9$) is far less prominent in the hotter dark stars. We conclude that while blackbody spectra may be useful for deriving order-of-magnitude estimates of *JWST* fluxes for the hotter dark stars, detailed stellar atmosphere models are required to accurately predict the fluxes for cool dark stars at high redshifts.

3.2. Dark Stars Magnified by Gravitational Lensing

Figures 1 and 2 demonstrate that all dark stars in Table 1 are *intrinsically* too faint at $z \geqslant 6$ to be detected by *JWST*, even if extremely long exposure times ($t_{\rm exp} = 3.6 \times 10^5$ s, i.e., 100 hr) are considered. The only hope of detecting isolated dark stars with *JWST* at these redshifts would then be to exploit the gravitational lensing provided by a foreground galaxy cluster. Galaxy clusters at $z \approx 0.1$–0.6 can in principle boost the fluxes of high-redshift objects by up to factors ~100 (e.g., Bradač et al. 2009; Maizy et al. 2010). As shown in Figure 2, this would be sufficient to lift some of the cooler ($T_{\rm eff} < 30,000$ K) dark star models above the *JWST* detection threshold. For each separate dark star model, the entries in the max($z_{\rm obs}$) column in Table 1 indicate the maximum redshifts at which 5σ detections are possible in at least one *JWST* filter after 3.6×10^5 (100 hr) exposures, assuming a magnification of $\mu = 160$ (see below). No dark stars are detectable at $z > 13$, even when this boost due to lensing is taken into account.

How many dark stars at $z \approx 10$ would one then expect to detect in a survey of a single lensing cluster? This depends on the magnification properties of the cluster, on the cosmic star formation history of dark stars, and on their typical lifetimes τ (which we treat as a free parameter bounded from above by $t_{\rm max}$, as discussed in Section 2: $0 \leqslant \tau \leqslant t_{\rm max}$). While gravitational lensing boosts the fluxes of background objects, their surface number densities are at the same time diluted by a factor equal to the magnification μ. In a region with angular area θ^2 and magnification μ, one can show that the expected number of dark stars $N_{\rm DS}$ in the redshift interval $[z_{\rm min}, z_{\rm max}]$ is given by

$$N_{\rm DS} = c\theta^2 \int_{z_{\rm min}}^{z_{\rm max}} \int_{t(z)}^{t(z)-\tau} \frac{{\rm SFR}(t)d_{\rm os}(z)^2(1+z)^3}{\mu(z)M_{\rm DS}} \frac{dt}{dz} dt\, dz, \quad (3)$$

where ${\rm SFR}(t)$ is the star formation rate (in units of $M_\odot$ Mpc^{-3} yr^{-1}) of dark stars at cosmic epoch $t(z)$, $M_{\rm DS}$ is the dark star mass (assumed to be the same for all such objects), and $d_{\rm os}(z)$ is the angular size distance between the observer and source at redshift z. In the case of flat ΛCDM cosmologies, the derivative $\frac{dt}{dz}$ in Equation (3) is given by:

$$\frac{dt}{dz} = -\frac{1}{H_0(1+z)[\Omega_M(1+z)^3 + \Omega_\Lambda]^{1/2}}. \quad (4)$$

When exploring the prospects of detecting isolated dark stars in the high-magnification regions of a foreground galaxy cluster, we have adopted MACS J0717.5+3745 at $z = 0.546$ as our

lensing cluster. This object has the largest angular Einstein radius detected so far, with a relatively shallow surface mass-density profile which boosts the projected area corresponding to high magnifications (Zitrin et al. 2009, 2010). Both of these properties combine to make this the best lens currently known for the study of faint objects at very high redshifts. For this cluster, the angular area over which the magnification is in the range $\mu = 100$–300 (with an average magnification $\overline{\mu} \approx 160$) for sources at $z_{\rm s} = 6$–20 is $\approx$0.3 arcmin^2.

For the cosmic star formation history SFR(t) of dark stars, we have explored three different scenarios from Trenti & Stiavelli (2009) for single population III stars forming through H$_2$ cooling in minihalos. These three scenarios differ in their assumptions concerning the amount of Lyman–Werner (hereafter LW) feedback expected during the relevant epochs. LW radiation is emitted by hot, high-mass stars, destroys H$_2$, and inhibits further population III star formation along this cooling channel. The very massive, fusion-driven population III stars that Spolyar et al. (2009) envision as the descendants of dark stars will emit copious amounts of LW radiation. However, if many of the population III stars that form through H$_2$ cooling (population III.1 stars in the notation suggested by Greif & Bromm 2006) go through a long-lived dark star phase (during which LW fluxes are insignificant due to the very low effective temperatures of these objects), this could substantially delay the onset of the LW feedback compared to scenarios with no dark stars. Hence, the amount of LW feedback at a given epoch is expected to depend both on the fraction $f_{\rm DS}$ of population III.1 stars that at some point become dark stars and on the typical duration τ of this phase.

The three scenarios from Trenti & Stiavelli (2009) that we consider are hereafter referred to as *standard LW*, *reduced LW*, and *no LW* and correspond to the cosmic star formation histories of population III stars formed through H$_2$ in minihalos depicted in their Figures 1, 2, and 3, respectively. The standard LW scenario, which we consider suitable for very small $f_{\rm DS}$ and short τ, pushes the bulk of population III star formation to higher redshifts than the other two (possibly more suitable for large $f_{\rm DS}$ and τ). Whereas all population III star formation has effectively ceased by $z \approx 10$ in the standard LW model, significant formation of such stars continues to lower redshifts in the other two scenarios.

In Figure 4, we plot the apparent AB magnitudes of selected dark star models versus the number of dark stars expected within the high-magnification regions ($\mu = 100$–300; $\overline{\mu} \approx 160$) of MACS J0717.5+3745 per unit redshift interval. These plots are based on the assumption of $f_{\rm DS} = 1$, i.e., that *all* population III stars formed through H$_2$ cooling in minihalos become dark stars and that all such dark stars display similar properties (in terms of mass, temperature, radius, and lifetime). In reality, this may not be very realistic. The individual merger history of each minihalo is likely to give rise to some variation in the central CDM density. Some minihalos may also host multiple stars (Turk et al. 2009; Stacy et al. 2010), which could cause some or all of the population III stars forming in such systems to wander out of the minihalo center where dark matter annihilation is the most efficient. The predictions in Figure 4 can, however, easily be rescaled to other dark star fractions by shifting the curves downward by a factor $f_{\rm DS}$.

The left column of Figure 4 displays the results for the 690 $M_\odot$, $T_{\rm eff} = 7500$ K dark star from the 1 GeV WIMP track, and the right column the corresponding results for the 716 $M_\odot$, $T_{\rm eff} = 23,000$ K dark star from the 100 GeV WIMP track.
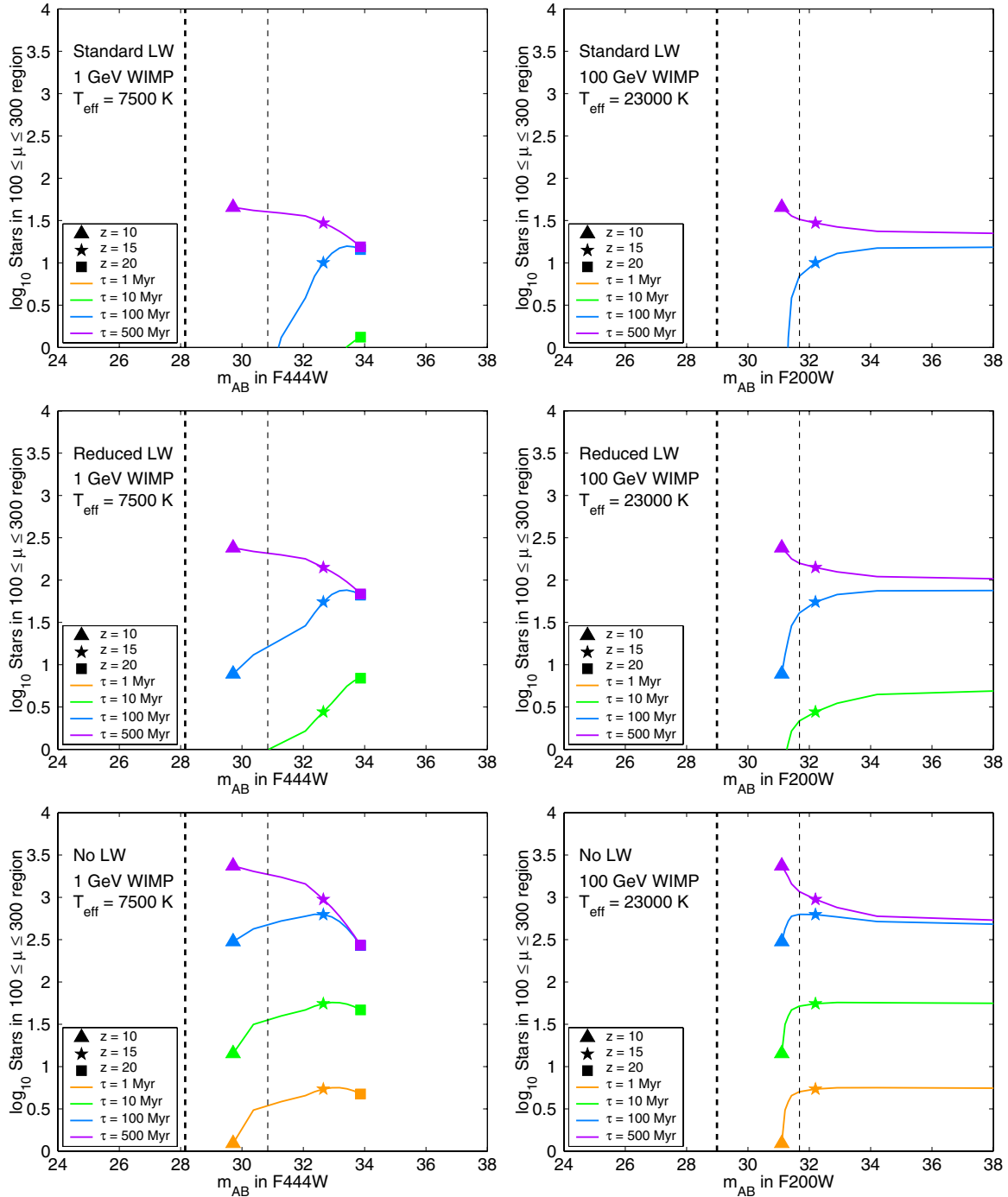
Figure 4. Number of dark stars per unit redshift interval predicted within the high-magnification regions ($\mu = 100$–300) of the galaxy cluster MACS J0717.5+3745, as a function of their apparent AB magnitudes in the *JWST*/NIRCam F444W (left column) and F200W (right column) filters. In the left column, the 690 $M_\odot$ dark star model with $T_{\rm eff} = 7500$ K from the 1 GeV WIMP track has been used, and in the right column the 716 $M_\odot$ dark star with $T_{\rm eff} = 23{,}000$ K the 100 GeV WIMP track. Within each panel, the differently colored lines correspond to dark star lifetimes of $\tau = 1$ Myr (orange; thin dot-dashed lines in the print version), 10 Myr (green; thin solid lines in the print version), 100 Myr (blue; thick dot-dashed lines in the print version), and 500 Myr (purple; thick solid lines in the print version). Symbols along these lines indicate dark star redshifts of $z = 10$ (triangle), $z = 15$ (star), and $z = 20$ (square). The different rows correspond to the standard LW (top row), reduced LW (middle row), and no LW (bottom row) star formation histories for population III stars in minihalos (Trenti & Stiavelli 2009). The vertical lines within each panel represent the *JWST* detection thresholds for 10σ detections after 10^4 s exposures (thick dashed) and 5σ detections after 3.6×10^5 s (100 hr) exposures (thin dashed). All population III stars forming through H$_2$ cooling in minihalos are here assumed to go through a dark star phase with identical properties, but the results can easily be generalized by scaling the curves downward by the dark star fraction $f_{\rm DS}$. The lines extending to the right hand borders of the plots reflect the sharply decreasing fluxes in the F200W filter due to foreground H I absorption in the intergalactic medium at $z > 15$.

(A color version of this figure is available in the online journal.)

Due to the different temperatures of these dark stars, the AB magnitudes in the NIRCam F444W filter are used in the left column and the NIRCam F200W filter in the right column. For both of these dark star models, the upper limit on the lifetime set by Equation (2) is $t_{\rm max} = 5 \times 10^8$ yr. For each model, we therefore consider lifetimes of $\tau = 10^6$ (orange lines; thin dot-

dashed lines in the print version), 10^7 (green lines; thin solid lines in the print version), 10^8 (blue lines; thick dot-dashed lines in the print version), and 5×10^8 yr (purple lines; thick solid lines in the print version). The three rows of panels in Figure 4 correspond to the cosmic population III star formation histories with standard LW (top row), reduced LW (middle row), and no LW feedback (bottom row). The different markers within each panel indicate the AB magnitudes and numbers of dark stars at redshifts $z = 10$ (triangle), $z = 15$ (star), and $z = 20$ (square).

In general, long dark star lifetimes τ imply larger numbers of dark stars at detectable brightnesses. In the case of the 690 $M_\odot$, $T_{\rm eff} = 7500$ K dark star (right column), considerable numbers ($\geqslant 10$) of dark stars are expected to be sufficiently bright for detection (at 5σ after 3.6×10^5 s) in the high-magnification regions of MACS J0717.5+3745 at $z \approx 10$–11, provided that their lifetimes are $\approx 5 \times 10^8$ yr. This holds true regardless of which of the three feedback scenarios is adopted. For the reduced LW and no LW feedback models, significant dark stars are expected even if the lifetime is closer to $\tau = 10^7$ yr. In the no LW scenario, even $\tau = 10^6$ yr dark stars can be detected behind MACS J0717.5+3745 but only in modest numbers (<10). The situation for the 716 $M_\odot$, $T_{\rm eff} = 23,000$ K dark star (right column) is similar, except that this model remains detectable up to a redshift of $z \approx 13$.

Dark stars with $\tau = 5 \times 10^8$ yr do not show the same decline in their expected numbers when going from $z = 15$ to $z = 10$ as dark stars with shorter lifespan do. This happens because $\tau = 5 \times 10^8$ yr dark stars have lifetimes that exceed the cosmic age intervals between adjacent redshift bins, allowing such objects to accumulate at lower redshifts, even though the cosmic star formation rate of population III stars is declining at these epochs for all three feedback scenarios. The Trenti & Stiavelli (2009) models do not allow us to trace the star formation history to epochs at $z < 10$, even though the star formation rate clearly remains non-zero at $z = 10$ in both the reduced LW and no LW feedback scenarios. In fact, $\tau = 5 \times 10^8$ yr dark stars forming at $z \geqslant 10$ in these feedback scenarios will survive in detectable numbers to even lower redshifts ($z \approx 6$), even if one artificially sets their formation rates to zero at $z < 10$.

In summary, cool ($T_{\rm eff} \leqslant 30,000$ K) and long-lived ($\tau \gtrsim 10^7$ yr) dark stars may well be detected at $z \approx 10$ in sizeable numbers within a single, ultra deep *JWST* field if one takes advantage of the magnifying power of a foreground galaxy cluster. In the case of high τ ($\gtrsim 10^8$ yr) and cosmic star formation scenarios, which imply significant dark star formation at $z < 15$, several dark stars may be seen even if only a minor fraction ($f_{\rm DS} \sim 0.01$–0.1) of all population III stars forming in minihalos become dark stars with temperatures in the detectable range.

4. DISCUSSION

4.1. How to Distinguish Isolated Dark Stars from Other Objects

As demonstrated in Section 3.2, certain varieties of $z \approx 10$ dark stars may be sufficiently bright and numerous to be detected by a *JWST*/NIRCam survey of the high-magnification regions of a foreground galaxy cluster. But how does one identify such objects among the overwhelming number of mundane interlopers located in front of, inside, or beyond the lensing cluster?

Given the many degeneracies involved in the interpretation of broadband photometry, there may well be unresolvable ambiguities in some cases. However, many of the cooler
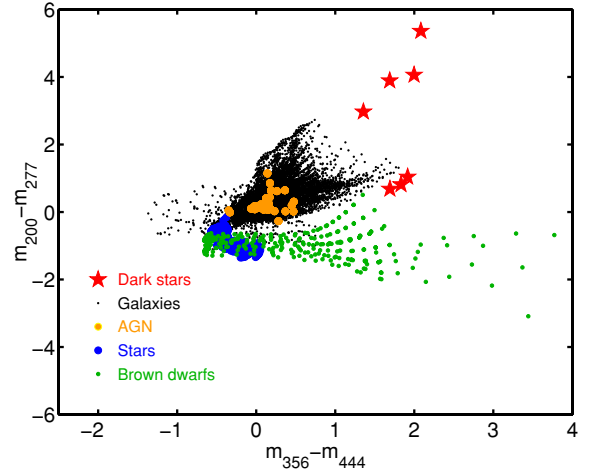

Figure 5. *JWST*/NIRCam $m_{356} - m_{444}$ vs. $m_{200} - m_{277}$ colors of $T_{\rm eff} <$ 10,000 K dark stars at $z = 10$ (red star symbols) compared to a number of potential interlopers in multiband surveys: star clusters or galaxies at $z = 0$–15 (black dots), AGN template spectra at $z = 0$–15 (yellow dots), Milky Way stars with $T_{\rm eff} = 2000$–50,000 K and $Z = 0.001$–0.020 (blue dots), and Milky Way brown dwarfs with $T_{\rm eff} = 130$–2200 K (green dots). Since the dark stars reside in a region of this color–color diagram that is disconnected from those occupied by these other objects, it should be possible to identify possible dark star candidates in deep multiband *JWST*/NIRCam surveys.

high-redshift dark stars should stand out in multiband survey data because of their unusual colors. This is demonstrated in Figure 5, where we plot the color indices $m_{356} - m_{444}$ versus $m_{200} - m_{277}$ (based on AB magnitudes in the *JWST*/NIRCam F200W, F277W, F356W, and F444W filters) at $z = 10$ for all dark stars from Table 1 with $T_{\rm eff} < 10,000$ K. The colors of these models (red star symbols) are compared to the colors predicted for a wide range of galaxies, star clusters, active galactic nuclei (AGNs), and Milky Way stars. The cloud of black dots in Figure 5 indicate the colors of integrated stellar populations (star clusters and galaxies) generated with the Zackrisson et al. (2001) spectral synthesis model. These predictions are based on instantaneous-burst,[13] Salpeter-IMF stellar populations at redshifts $z = 0$–15 with metallicities in the range $Z = 0.001$–0.020, ages ranging from 10^6 yr up to the age of the universe at each redshift, and a rest-frame stellar dust reddening of $E(B - V) = 0$–0.5 mag assuming the Calzetti et al. (2000) extinction law. Also included in Figure 5 are the expected colors of foreground stars with $T_{\rm eff} = 2000$–50,000 K and $Z = 0.001$–0.020 in the Milky Way (i.e., at $z = 0$) based on the Lejeune et al. (1998) compilation of synthetic stellar atmosphere spectra (blue dots), and the colors of Milky Way brown dwarfs in the 130–2200 K range based on the Burrows et al. (2003, 2006) models (green dots). The yellow dots represent the template AGN spectra of Hopkins et al. (2007) for bolometric luminosities $\log_{10} L_{\rm bol}/L_\odot = 8.5$–14.0, at redshifts $z = 0$–15. Since none of these potential interlopers have $m_{356} - m_{444}$ and $m_{200} - m_{277}$ colors that overlap with those of cool $z \approx 10$ dark stars, a diagnostic diagram of this type can be used to cull objects that are clearly *not* dark stars from multiband survey data. However, given that $T_{\rm eff} < 10,000$ K dark stars are unlikely to attain apparent magnitudes brighter than $m_{\rm AB} \approx 30$ at their peak wavelengths (even when boosted by gravitational lensing; see Figure 2(b)) and can realistically only be detected

---

[13] This is a conservative choice, since allowing for more extended star formation histories would only result in a more restricted color coverage for these objects.
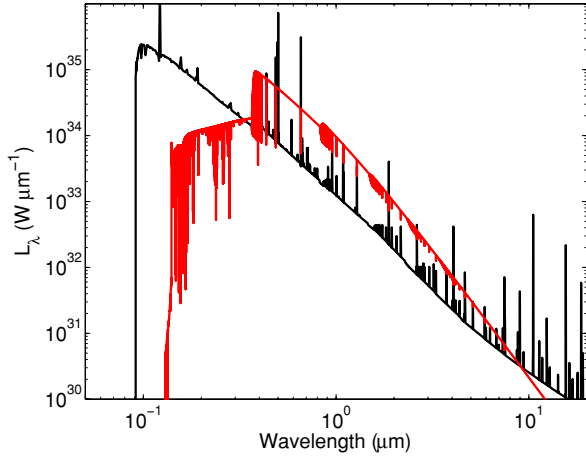
Figure 6. Rest-frame spectrum of a $10^6 \, M_\odot$, $Z = 0.001$, Salpeter-IMF stellar population (stellar mass range 0.08–120 $M_\odot$) which has formed stars at a constant rate for 10^8 yr (black line) with a superimposed contribution (red line) from ten $T_{\rm eff} = 7500$ K, 690 $M_\odot$ dark stars (from the 1 GeV WIMP track). Despite making up only 0.7% of the stellar mass in this galaxy, these dark stars give rise to an upturn in the spectrum at rest-frame wavelengths longward of $0.36 \, \mu$m. In a $z = 10$ object, this spectral feature should appear longward of $3.96 \, \mu$m and could serve as a telltale signature of cool dark stars within the first galaxies. Due to the low but non-zero metallicity ([Fe/H] = −5) of the MARCS model for the 690 $M_\odot$ dark stars, numerous metal absorption lines are seen throughout the red spectrum. While these lines appear to be strong due to the high spectral resolution of the model, they actually have very small equivalent widths and negligible impact on the *JWST* broadband fluxes.

in one or two NIRCam filters, follow-up spectroscopy of the remaining dark star candidates will be required to establish their exact nature. This will admittedly be very challenging, but a very coarse spectrum can possibly be obtained for $m_{\rm AB} \approx 30$ objects with *JWST*/NIRSpec (assuming a 3.6×10^5 s exposure). Objects of this type may also be suitable targets for the 42 m European Extremely Large Telescope[14].

4.2. The Spectral Signature of Dark Stars in High-redshift Galaxies

The first galaxies are expected to form at $z \approx 10$–13 in CDM halos with total masses around $10^8 \, M_\odot$ (e.g., Johnson et al. 2008, 2009; Greif et al. 2008; Ricotti 2010). At the time of assembly, each such object is likely to contain a number of minihalos in which population III stars have already formed (Greif et al. 2008). If some of these population III stars go through a long-lived ($\tau \gtrsim 10^8$ yr) dark star phase, several dark stars may in principle congregate inside the first generation of galaxies and give rise to telltale signatures in their integrated spectra. In Figure 6, we display the rest-frame spectrum predicted by the Zackrisson et al. (2001) population synthesis model for a 10^8 yr old, low-metallicity ($Z = 0.001$, i.e., population II), Salpeter-IMF (mass range 0.08–120 $M_\odot$) stellar population which has formed stars at a constant rate. This population has been assigned a stellar mass of $10^6 \, M_\odot$, which—for a $10^8 \, M_\odot$ halo with baryon fraction $f_{\rm bar} \approx 0.7$—corresponds to ~10% of the baryonic mass in stars, in rough agreement with the models of Ricotti (2010) for a $z \approx 10$ galaxy. The predicted NIRCam magnitudes of this object lie around $m_{\rm AB} \approx 33$–34 which would make it sufficiently bright for detection with *JWST* if seen through a gravitational lens with magnification $\mu \gtrsim 10$. Superposed on the spectrum of this high-redshift galaxy is the integrated contribution from ten $T_{\rm eff} = 7500$ K (the 690 $M_\odot$ models from the 1 GeV WIMP track)
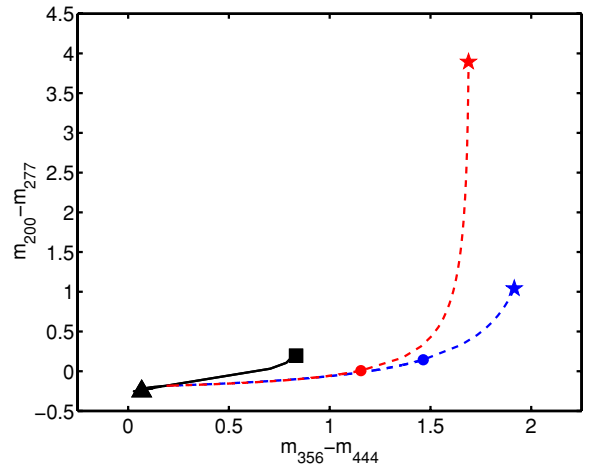
Figure 7. *JWST*/NIRCam $m_{356} - m_{444}$ vs. $m_{200} - m_{277}$ color evolution as a function of age for a $z = 10$, low-metallicity ($Z = 0.001$), Salpeter-IMF galaxy experiencing a short burst of star formation (10^8 yr) and passive evolution thereafter (black line). The black triangle indicates an age of 10^6 yr and the black square 5×10^8 yr (roughly the age of the universe at this redshift). The star symbols indicate the colors of two cool, $z = 10$ dark stars from Table 1: the 7500 K, 690 $M_\odot$ model from the 1 GeV WIMP track (blue star) and the 5800 K, 106 $M_\odot$ model from the 100 GeV WIMP track (red star). Both of these (as is the case for all $T_{\rm eff} < 10,000$ K dark stars observed in these filters; see Figure 5) are considerably redder than the colors expected for galaxies, regardless of their age. Dashed lines indicate how the colors of the model galaxy (at an assumed age of 10^8 yr) would shift if it were to contain dark stars of either of the two types. The filled circles along the dashed tracks indicate mixtures at which these dark stars make up 1% of the stellar mass in the model galaxy. These points are also significantly redder than the reddest point along the galaxy track, indicating that an ~1% stellar mass fraction in dark stars within $z \approx 10$ galaxies would be detectable through multiband photometry.

dark stars (red line). These dark stars, which contribute only 0.7% of the stellar mass in this galaxy, give rise to a conspicuous red bump in the spectrum at rest-frame wavelengths longward of $0.36 \, \mu$m (this corresponds to wavelengths longer than $3.96 \, \mu$m at $z = 10$). Because of this, galaxies that contain many cool dark stars are expected to display anomalously red colors. A feature like this is very difficult to produce through other means. For instance, the spectrum depicted in Figure 6 cannot be attributed to dust reddening, since no known extinction law would allow a sharp rise in flux at wavelengths longward of $0.36 \, \mu$m to coexist with a very blue continuum at shorter wavelengths. Attributing the red bump as due to thermal dust emission is also untenable, since this would require dust radiating at a temperature close to that of the dark star (7500 K), which is higher than the sublimation temperature of all known types of dust.

In Figure 7, we display the $m_{356} - m_{444}$ versus $m_{200} - m_{277}$ color evolution (black solid line) as a function of age for the synthetic galaxy from Figure 6 at $z = 10$. Here, the age runs from 10^6 yr (black triangle) up to the age of the universe at this redshift ($\approx 5 \times 10^8$ yr). Also indicated are the colors of two cool dark stars: the 7500 K model from the 1 GeV WIMP track (blue star) and the 5800 K model from the 100 GeV WIMP track (red star). Due to their low temperatures, these two dark stars are far redder than the model galaxy in both colors plotted. As shown in Figure 5, this is generally the case for $T_{\rm eff} < 10,000$ K dark stars observed in these filters. The galaxy is here assumed to go through a short burst of star formation (forming stars at a constant rate for 10^8 yr), after which it evolves passively. This gives a conservative estimate of the color difference between galaxies and dark stars. Allowing a more extended star formation episode or a star formation rate that increases over time would

only increase the discrepancy between the colors of dark stars and the model galaxy. The dashed lines indicate how the colors of a 10^8 yr galaxy would shift in this diagram, if it were to harbor dark stars of the type considered. The filled circles along each such mixing track indicate the position at which the dark stars make up 1% of the total stellar mass. Since these points are significantly redder in the $m_{356} - m_{444}$ color than the reddest point along the standard galaxy track, an $\sim$1% stellar mass fraction in dark stars would result in very peculiar colors for $z = 10$ galaxies and should allow such objects to be identified as candidate "dark star galaxies" in *JWST* multiband survey data.

5. SUMMARY

In this paper, we have investigated the prospects of detecting very massive, high-redshift dark stars using the *JWST*. While individual dark stars at $z > 6$ will be intrinsically too faint for detection, we demonstrate that the magnification provided by a foreground galaxy cluster will make certain varieties of long-lived ($\tau \geqslant 10^7$ yr) and cool ($T_{\rm eff} \leqslant 30{,}000$ K) detectable at redshifts up to $z \approx 10$. We argue that it should be possible to identify at least some of these dark stars in photometric NIRCam surveys due to their peculiar colors. If the lifetimes of dark stars are sufficiently long, they may also congregate during the hierarchical assembly of the first galaxies. We find that this could give rise to distinct signatures in the integrated NIRCam colors of high-redshift galaxies, provided that dark stars make up at least $\sim$1% of the overall stellar mass in these objects.

REFERENCES

Abbasi, R., et al. 2009, Phys. Rev. Lett., 102, 201302
Abel, T., Bryan, G. L., & Norman, M. L. 2002, Science, 295, 93
Ahmed, Z., et al. 2009, Phys. Rev. Lett., 102, 011301
Bradač, M., et al. 2009, ApJ, 706, 1201
Bromm, V., Coppi, P. S., & Larson, R. B. 2002, ApJ, 564, 23
Bromm, V., Kudritzki, R. P., & Loeb, A. 2001, ApJ, 552, 464
Burrows, A., Sudarsky, D., & Hubeny, I. 2006, ApJ, 640, 1063
Burrows, A., Sudarsky, D., & Lunine, J. I. 2003, ApJ, 596, 587
Calzetti, D., Armus, L., Bohlin, R. C., Kinney, A. L., Koornneef, J., & Storchi-Bergmann, T. 2000, ApJ, 533, 682
Casanellas, J., & Lopes, I. 2009, ApJ, 705, 135
Cooray, A., et al. 2009, in astro2010: The Astronomy and Astrophysics Decadal Survey, 54
Cox, A. N., (ed.) 2000, Allen's Astrophysical Quantities (New York: Springer)
Dijkstra, M., & Wyithe, J. S. B. 2007, MNRAS, 379, 1589
Fairbairn, M., Scott, P., & Edsjö, J. 2008, Phys. Rev. D, 77, 047301
Fan, X., et al. 2006, AJ, 132, 117
Freese, K., Bodenheimer, P., Spolyar, D., & Gondolo, P. 2008, ApJ, 685, L101
Freese, K., Gondolo, P., Sellwood, J. A., & Spolyar, D. 2009, ApJ, 693, 1563
Freese, K., Ilie, C., Spolyar, D., Valluri, M., & Bodenheimer, P. 2010, ApJ, submitted (arXiv:1002.2233)
Freese, K., Spolyar, D., & Aguirre, A. 2008, J. Cosmol. Astropart. Phys., JCAP11(1997)014
Greif, T. H., & Bromm, V. 2006, MNRAS, 373, 128
Greif, T. H., Johnson, J. L., Klessen, R. S., & Bromm, V. 2008, MNRAS, 387, 1021
Gustafsson, B., Edvardsson, B., Eriksson, K., Jørgensen, U. G., Nordlund, Å., & Plez, B. 2008, A&A, 486, 951
Heger, A., Woosley, S., Baraffe, I., & Abel, T. 2002, in ESO Astrophys. Symp., Lighthouses of the Universe: The Most Luminous Celestial Objects and Their Use for Cosmology, ed. M. Gilfanov, R. Sunyaev, & E. Churazov (Berlin: Springer), 369
Hopkings, P. F., Richards, G. T., & Hernquist, L. 2007, ApJ, 654, 731
Hubeny, I., & Lanz, T. 1995, ApJ, 439, 875
Iocco, F. 2008, ApJ, 677, L1
Iocco, F. 2009, Nucl. Phys. Proc. Suppl., 194, 82
Iocco, F., Bressan, A., Ripamonti, E., Schneider, R., Ferrara, A., & Marigo, P. 2008, MNRAS, 390, 1655
Iocco, F., Mangano, G., Miele, G., Pisanti, O., & Serpico, P. D. 2007, Phys. Rev. D, 75, 087304
Johnson, J. L. 2010, MNRAS, 404, 1425
Johnson, J. L., Greif, T. H., & Bromm, V. 2008, MNRAS, 388, 26
Johnson, J. L., Greif, T. H., Bromm, V., Klessen, R. S., & Ippolito, J. 2009, MNRAS, 399, 37
Lejeune, T., Cuisinier, F., & Buser, R. 1998, A&AS, 130, 65
Madau, P. 1995, ApJ, 441, 18
Maizy, A., Richard, J., De Leo, M. A., Pelló, R., & Kneib, J. P. 2010, A&A, 509, 105
Natarajan, A., Tan, J. C., & O'Shea, B. W. 2009, ApJ, 692, 574
Ricotti, M. 2010, Advances in Astronomy, 2010, 1
Ripamonti, E., Iocco, F., Bressan, A., Schneider, R., Ferrara, A., & Marigo, P. 2009, Proc. Identification of Dark Matter 2008, PoS IDM2008:075,2009
Ripamonti, E., Iocco, F., Bressan, A., Schneider, R., Ferrara, A., & Marigo, P. 2010, MNRAS, in press (arXiv:1003.0676)
Salati, P., & Silk, J. 1989, ApJ, 338, 24
Santos, M. R., Bromm, V., & Kamionkowski, M. 2002, MNRAS, 336, 1082
Savage, C., Gelmini, G., Gondolo, P., & Freese, K. 2009, J. Cosmol. Astropart. Phys., JCAP04(1997)010
Scannapieco, E., Schneider, R., & Ferrara, A. 2003, ApJ, 589, 35
Schaerer, D. 2002, A&A, 382, 28
Schaerer, D. 2003, A&A, 397, 527
Schleicher, D. R. G., Banerjee, R., & Klessen, R. S. 2009, Phys. Rev. D, 79, 3510
Scott, P., Edsjö, J., & Fairbairn, M. 2008, in Dark Matter in Astroparticle and Particle Physics: Dark 2007, ed. H. K. Klapdor-Kleingrothaus & G. F. Lewis (Singapore: World Scientific), 387
Scott, P., Edsjö, J., & Fairbairn, M. 2009a, arXiv:0904.2395
Scott, P., Fairbairn, M., & Edsjö, J. 2009b, MNRAS, 394, 82
Scott, P., & Sivertsson, S. 2009, Phys. Rev. Lett., 103, 211301
Sokasian, A., Yoshida, N., Abel, T., Hernquist, L., & Springel, V. 2004, MNRAS, 350, 47
Spolyar, D., Bodenheimer, P., Freese, K., & Gondolo, P. 2009, ApJ, 705, 1031
Spolyar, D., Freese, K., & Gondolo, P. 2008, Phys. Rev. Lett., 100, 051101
Stacy, A., Greif, T. H., & Bromm, V. 2010, MNRAS, 403, 45
Taoso, M., Bertone, G., Meynet, G., & Ekström, S. 2008, Phys. Rev. D, 78, 13510
Tegmark, M., Silk, J., Rees, M. J., Blanchard, A., Abel, T., & Palla, F. 1997, ApJ, 474, 1
Trenti, M., & Stiavelli, M. 2009, ApJ, 694, 879
Trenti, M., Stiavelli, M., & Shull, M. 2009, ApJ, 694, 879
Tumlinson, J., & Shull, J. M. 2000, ApJ, 528, L65
Turk, M. J., Abel, T., & O'Shea, B. 2009, Science, 325, 601T
Umeda, H., Yoshida, N., Nomoto, K., Tsuruta, S., Sasaki, M., & Ohkubo, T. 2009, J. Cosmol. Astropart. Phys., JCAP08(2009)024
Weinmann, S. M., & Lilly, S. J. 2005, ApJ, 624, 526
Yoon, S.-C., Iocco, F., & Akiyama, S. 2008, ApJ, 688, L1
Yoshida, N., Abel, T., Hernquist, L., & Sugiyama, N. 2003, ApJ, 592, 645
Zackrisson, E., Bergvall, N., Olofsson, K., & Siebert, A. 2001, A&A, 375, 814
Zitrin, A., Broadhurst, T., Barkana, R., Rephaeli, Y., & Benitez, N. 2010, MNRAS, submitted (arXiv:1002.0521)
Zitrin, A., Broadhurst, T., Rephaeli, Y., & Sadeh, S. 2009, ApJ, 707, L102